Intramolecular Hydrogen Atom Tunneling in 2-Chlorobenzoic Acid Studied by Low-Temperature Matrix-Isolation Infrared Spectroscopy

Satoshi Nishino and Munetaka Nakata*

Graduate School of BASE (Bio-Applications and Systems Engineering), Tokyo University of Agriculture and Technology, Naka-cho, Koganei, Tokyo 184-8588, Japan

Received: March 4, 2007; In Final Form: May 10, 2007

Intramolecular hydrogen atom tunneling in 2-chlorobenzoic acid has been investigated by low-temperature matrix-isolation infrared spectroscopy with the aid of density functional theory calculation. Infrared spectra of two relatively stable *syn* isomers, SC and ST, were observed in argon and xenon matrixes. When the matrix samples were annealed after deposition, the isomerization from ST to SC occurred around the benzene−carboxyl bond. Two less stable *anti* isomers, AT, which has an OH···Cl intramolecular hydrogen bond, and AC, which has no OH···Cl bond, were produced from SC and ST upon UV irradiation. When the matrix samples were kept in the dark after UV irradiation, AT and AC changed to ST and SC, respectively, by spontaneous isomerization around the C−O axis in the carboxyl group. The rate constants of isomerization, AT → ST, in a Xe matrix were estimated from the absorbance changes at various matrix temperatures. The rate constants showed a drastic decrease in deuteration of the hydrogen atom of the carboxyl group. The relationship between the rate constants and the matrix temperature did not follow the Arrhenius law. These findings lead to the conclusion that the isomerization of AT → ST and AC → SC in low-temperature rare-gas matrixes proceeds through intramolecular hydrogen atom tunneling.

Introduction

It is one of the important subjects in physical chemistry and biochemistry to clarify the role of hydrogen atom tunneling in the isomerization around the C−O bonds of alcohols and acids. A number of recent rare-gas matrix-isolation studies have shown that isomerization through hydrogen tunneling occurs in aliphatic carboxylic acids such as formic acid,[1−3] acetic acid,[1,4,5] and propionic acid.[1,6] As shown in Scheme 1, at least two isomers, *syn* and *anti*, are conceivable for these acids, where the latter is less stable because of the repulsion between the nonbonded electron pairs of two oxygen atoms in the carboxyl group. It was concluded that the more stable isomer, *syn*, for the above-mentioned compounds changed to the corresponding less stable isomer, *anti*, upon infrared (IR) irradiation and then returned to the original isomer in the dark through hydrogen tunneling. Similar isomerization due to hydrogen tunneling after UV-induced isomerization was reported on aromatic alcohols and acids such as hydroquinone,[7] chloranilic acid,[8] and tetrachlorohydroquinone[9] in low-temperature rare-gas matrixes.

It seems to be important to study the hydrogen tunneling in molecules containing intramolecular hydrogen bonds, which causes a significant change on the asymmetric potential surfaces in relation to both *syn* and *anti* isomers. For example, the *anti* instead of *syn* isomer of 2-chloroacetic acid is stabilized by intramolecular OH···Cl bonding, lowering the energy difference between the two isomers. Then the barrier of isomerization from the *anti* isomer is raised too high to induce the isomerization through hydrogen tunneling in the dark,[10−12] in contrast to acetic acid, a parent molecule for 2-chloroacetic acid, which shows isomerization due to the hydrogen tunneling.

In the present study, the isomerization of 2-chlorobenzoic acid, hereafter denoted as 2CBA, has been examined by low-temperature rare-gas matrix-isolation IR spectroscopy and density functional theory (DFT) calculation. Benzoic acid, a parent molecule of 2CBA, was studied by electron diffraction in the gas phase[13] and in rare-gas matrixes by IR spectroscopy,[14,15] where only the *syn* isomer was detectable. These results seem to be reasonable because the *anti* isomer is destabilized by repulsion between the two hydrogen atoms of the OH group and the benzene ring, as shown in Scheme 2. The potential energy of the *anti* isomer increases, and then the barrier height of isomerization from the *anti* isomer becomes smaller and facilitates the tunneling isomerization. Therefore, even if the *anti* isomer is produced upon IR and/or vis−UV irradiation, it would immediately change to the *syn* isomer through hydrogen tunneling. The lifetime of the less stable isomer should be too short to be detectable by electron diffraction or standard IR spectroscopy, as mentioned above.

If this explanation is true, the *anti* isomer of 2CBA, which is stabilized by the OH···Cl intramolecular hydrogen bond, should be detectable because the tunneling rate is slower, i.e., the lifetime of the *anti* isomer is longer, than that of benzoic acid. In fact, a few IR bands of a less stable isomer for 2CBA in the

SCHEME 1

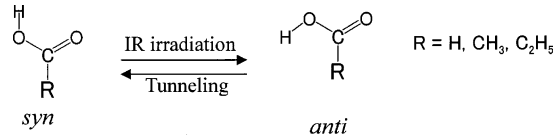

SCHEME 2

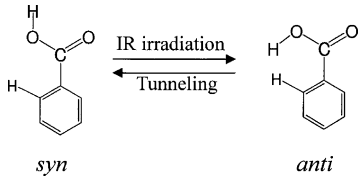

* To whom correspondence should be addressed. Fax: +81-42-388-7349. E-mail: necom@cc.tuat.ac.jp.

10.1021/jp0717600 CCC: $37.00 © 2007 American Chemical Society
Published on Web 06/28/2007

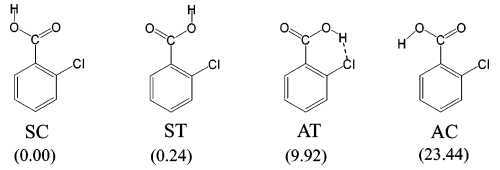

Figure 1. Four isomers of 2-chlorobenzoic acid optimized at the DFT/B3LYP/6-31++G** level. The numbers in parentheses represent the relative energies (kJ mol^{-1}). The broken line represents an intramolecular hydrogen bond.

C═O and O−H stretching regions were observed in CCl_4 solution[16] or in the gas phase.[17] However, no report on the mechanism of photoisomerization or tunneling isomerization has yet been investigated.

In the present study, we first examine the UV-induced photoisomerization of 2CBA to identify four possible isomers including two less stable isomers that have never been reported (see Figure 1). Then we study the tunneling isomerization from the less stable isomers to the more stable isomers. The rate constants of isomerization for the normal and deuterated samples are determined in kinetic analyses at various matrix temperatures. The dependence of the rate constants on the matrix temperature and the H/D isotope effect on the rate constants have provided us with a clue as to the mechanism of the isomerization caused by hydrogen tunneling.

Experimental and Calculation Methods

A sample of 2CBA was purchased from Tokyo Chemical Industry Co. Ltd. A deuterated sample of 2-CBA−OD was synthesized by mixing 2CBA in acetone with an excess amount of D_2O. A solid sample of normal or deuterated species dried in a glass vacuum system was placed in a stainless steel pipe nozzle with a heating system. Pure Ar (Taiyo Toyo Sanso, 99.9999% purity) or Xe (Tokyo Gas Chemical, 99.999%) was flowed over the sample heated to ca. 320 K, where the flow rate of the rare gas was adjusted by a needle valve to obtain a suitable sample/rare gas ratio. The mixed gas was expanded through a stainless steel pipe and deposited in a vacuum chamber on a CsI plate cooled at 9 K by a closed-cycle helium refrigerator (Iwatani, model CW303). Matrix samples were warmed at a rate of 1 K/1 min, held for 10 min at 27 K, and then cooled to 9 K at the same rate in annealing. UV radiation from a super-high-pressure mercury lamp (Ushio, SX-UI-500HQ) was used to induce photoisomerization. A water filter was used to remove thermal reactions, and an LU0250 short-wavelength cutoff filter (Asahi Spectra Co. Ltd.) was used to select the irradiation wavelength (λ > 240 nm). IR spectra of the matrix sample and spectral changes due to photoisomerization and tunneling isomerization were measured with an FTIR spectrophotometer (JEOL, JIR-WINSPEC50). The spectral resolution was 0.5 cm^{-1}, and the accumulation number was 64. Other experimental details are reported elsewhere.[18,19]

DFT calculations were performed using the Gaussian03 program[20] with the 6-31++G** basis set. Beck's three-parameter hybrid density functional,[21] in combination with the Lee−Yang−Parr correlation functional (B3LYP),[22] was used to optimize the geometrical structures and to obtain IR spectral patterns.

Results and Discussion

Optimized Geometries. The four isomers of 2CBA, shown in Figure 1, were optimized at the DFT/B3LYP/6-31++G** calculation level. We call these isomers SC, ST, AT, and AC,

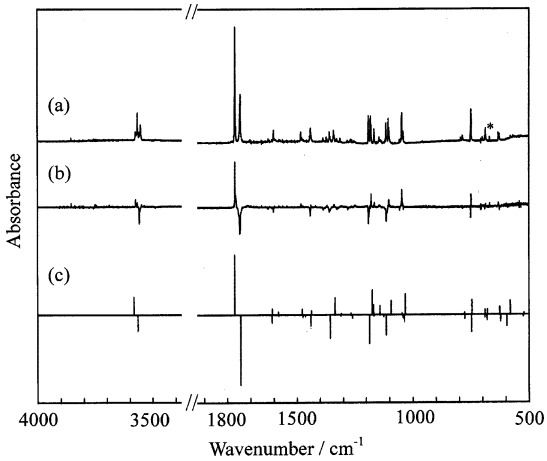

Figure 2. IR spectra of 2-chlorobenzoic acid in an argon matrix. (a) Observed spectrum after deposition. The band marked with an asterisk is due to CO_2 in the atmosphere. (b) Difference spectrum between the spectra measured after and before annealing. (c) Calculated spectral patterns of SC (up) and ST (down), where scaling factors of 0.95 and 0.98 are used inside and outside the OH stretching region, respectively.

where the former letter, *syn* (S) or *anti* (A), means the conformation of the hydrogen atom of OH against the oxygen atom of the carboxyl group, and the second letter, *cis* (C) or *trans* (T), means that of the oxygen atom of the carboxyl group against the chlorine atom. The optimized geometrical structures of SC, ST, and AC were found to be nonplanar, the dihedral angles of which are calculated to be 11.5°, 162.5°, and 53.9°, respectively. On the other hand, the geometrical structure of AT is planar, probably because of the OH···Cl hydrogen bond. Böhm reported the dihedral angles of SC and ST to be 20° and 157°, respectively, at the DFT/B3LYP/6-311++G** level,[16] which are consistent with the results of our calculation. A similar calculation was performed for 2-fluorobenzoic acid, 2FBA, by Nandi,[23] who reported that the carboxyl groups of the two *syn* isomers were in the plane of the benzene ring. Since the fluorine atom is far from the oxygen atom in 2FBA, the repulsion between the fluorine and oxygen atoms seems to be negligible. In contrast, the two *syn* isomers of 2CBA are nonplanar, which indicates that the distance between the oxygen and chlorine atoms in 2CBA is so close that the repulsion between these atoms cannot be ignored.

It is found that SC is the most stable isomer. The energies of ST, AT, and AC relative to SC are calculated to be 0.24, 9.92, and 23.44 kJ mol^{-1}, respectively. The two *anti* isomers, AT and AC, are less stable than the two *syn* isomers, SC and ST, as described in the Introduction by the repulsion between the lone pairs of the two oxygen atoms in the carboxyl group, although AT is stabilized by the intramolecular hydrogen bond. Then the order of relative energies for the four isomers shown in Figure 1, SC < ST < AT < AC, seems to be reasonable.

IR Spectra of SC and ST in Rare-Gas Matrixes. An IR spectrum of 2CBA in an argon matrix is shown in Figure 2a. Two C═O stretching bands clearly appear in the region of 1700−1800 cm^{-1}, implying the existence of two isomers. Judging from the populations calculated with an assumption of the Boltzmann distribution law using the above-mentioned relative energies, all the bands appearing in the spectrum can be assigned to the more stable isomers SC and ST but neither AT nor AC.

To distinguish the two *syn* isomer bands, the matrix sample was annealed from 9 to 27 K. A difference spectrum between the spectra measured before and after the annealing is shown in Figure 2b, where the scale of absorbance is expanded by 3

TABLE 1: Observed and Calculated Wavenumbers (cm^{-1}) and Relative Intensities of SC and ST in an Argon Matrix

SC						ST					
normal			deuterated			normal			deuterated		
	calcd[b]			calcd[b]			calcd[b]			calcd[b]	
obsd[a]	$\tilde{\nu}$	int	obsd[a]	$\tilde{\nu}$	int	obsd[a]	$\tilde{\nu}$	int	obsd[a]	$\tilde{\nu}$	int
3574, 3565 (s)	3581	30		3076	1	3557, 3551 (s)	3565	23		3065	1
	3076	0		3061	1		3065	1		3060	1
	3061	1		3048	3		3060	0		3047	2
	3049	3		3034	1		3048	2		3033	1
	3034	1	2637, 2627 (s)	2687	19		3034	1	2624, 2619 (s)	2674	15
1766 (s)	1767	100	1762, 1754 (s)	1760	100	1744 (s)	1742	100	1738 (vs)	1734	100
1597 (w)	1607	10	1598 (w)	1607	10	1602 (w)	1608	11	1601 (w)	1607	12
	1579	5		1579	5		1577	1		1577	1
1481 (w)	1476	10	1481 (w)	1476	10		1474	3		1473	4
1438 (w)	1438	7	1435 (w)	1438	7	1441 (m)	1440	16	1441 (w)	1439	15
1341 (w)	1335	29	1312 (s)	1321	18	1360 (m)	1356	33	1331 (s)	1320	55
	1308	2		1273	38		1310	1	1326 (s)	1307	25
	1266	3	1262 (s)	1263	37		1260	4		1254	1
1179, 1176 (s)	1173	41		1168	1	1187 (s)	1185	41		1166	0
1162 (m)	1167	16	1144 (w)	1142	4		1166	1		1127	1
1143 (w)	1140	15	1104 (w)	1100	6		1124	3	1125 (m)	1121	12
1103, 1101, 1098 (s)	1092	23		1046	3	1113 (s)	1113	29	1055 (w)	1042	4
	1047	3	1048 (s)	1033	25	1055 (w)	1042	4	1040 (w)	1036	7
1048 (s)	1032	35		986	2	1041 (w)	1036	9	999 (m)	991	15
	985	0	987 (w)	981	23		986	0		986	0
	959	0		959	1		964	0		964	0
	869	0		869	0		871	0		871	0
	790	0		788	1		789	0		788	1
	777	4		759	3		776	6	765 (w)	756	6
749, 747 (s)	745	25	749, 747 (s)	744	22	751 (s)	747	25	750 (w)	745	20
686 (w)	688	8		681	4	688 (w)	689	4		681	2
	678	9		664	4	678 (w)	680	8		665	2
631 (m)	625	13	596 (w)	588	18	626 (m)	622	10	593 (w)	585	13
	581	23		521	4		596	16		527	4
	521	3		492	16		525	3		492	18
	489	1		459	15		485	0		461	15
	442	1		435	6		447	3		444	14

[a] The symbols in parentheses represent the relative intensities: s, m, and w denote strong, medium, and weak, respectively. [b] Calculated at the DFT/B3LYP/6-31++G** level. Scaling factors of 0.95 and 0.98 are used in the regions higher and lower than 3000 cm^{-1}, respectively.

times that in Figure 2a. Figure 2c shows the calculated spectral patterns obtained by the DFT calculation, where the peaks of SC and ST are drawn on the upper and lower sides, respectively. The scaling factor of 0.95 is used for the OH stretching in consideration of anharmonicity and 0.98 otherwise. Since the observed difference spectrum, Figure 2b, is consistent with the calculated spectral pattern, Figure 2c, it can be concluded that the second stable isomer ST changes to the most stable isomer SC by the annealing. Then almost all the peaks appearing in Figure 2a are clearly assigned to SC and ST, as listed in Table 1. These assignments support the assumption proposed by Barnes[24] that thermal rotational isomerization around a single bond occurs over a barrier height lower than 8 kJ mol^{-1} at a matrix temperature higher than 27 K; the barrier height from ST to SC is estimated to be 7.51 kJ mol^{-1} in our calculation.

A deuterated sample was used to assess the reliability of our vibrational assignments. Figure 3a shows an IR spectrum for deuterated 2-CBA in an Ar matrix, where the D/H isotope ratio is 50−70% and the IR bands of normal species are subtracted from the observed spectrum computationally. The observed increasing and decreasing bands in the difference spectrum between the spectra measured before and after annealing, Figure 3b, can be assigned to the deuterated SC and ST isomers, because the corresponding calculated spectral patterns shown in Figure 3c reproduce the observed spectrum as closely as those for the normal species. The observed and calculated wavenumbers and relative intensities of deuterated SC and ST are summarized in Table 1 together with those of the normal species.

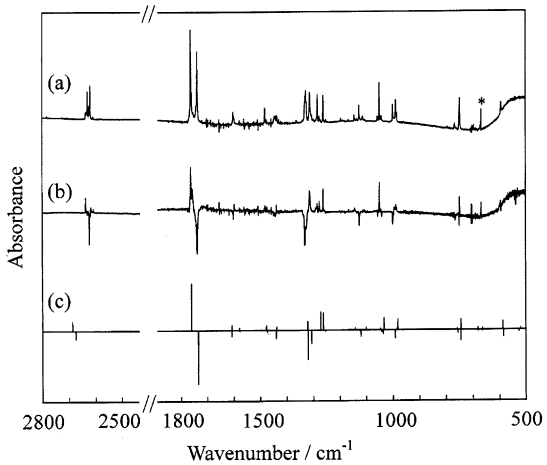

Figure 3. IR spectra of deuterated species of 2-chlorobenzoic acid in an argon matrix. (a) Observed spectrum after deposition. The band marked with an asterisk is due to CO_2 in the atmosphere. (b) Difference spectrum between the spectra measured after and before annealing. (c) Calculated spectral patterns of deuterated SC (up) and deuterated ST (down), where a scaling factor of 0.98 is used. The observed bands of the normal species are subtracted computationally.

IR Spectra of AT and AC Produced upon UV Irradiation. To observe the IR spectra of less stable unknown isomers, the matrix sample was exposed to UV radiation emitted from a super-high-pressure mercury lamp through an LU0250 short-cutoff filter (λ > 240 nm) after annealing. A difference IR

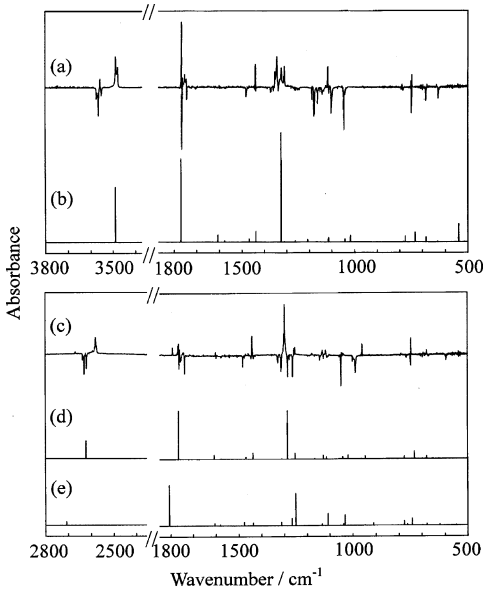

Figure 4. Spectral changes due to photoisomerization of 2-chlorobenzoic acid in an argon matrix. (a) Difference spectrum of the normal species between the spectra measured after and before 60 min of UV irradiation after annealing. (b) Calculated spectral pattern of AT. (c) Difference spectrum of deuterated species between the spectra measured after and before 60 min of UV irradiation. (d, e) Calculated spectral patterns of deuterated AT and deuterated AC, respectively.

spectrum between the spectra measured after and before the 60 min irradiation is shown in Figure 4a, where the product bands increase and the reactant bands, i.e., SC and ST, decrease. Figure 4b shows the calculated spectral pattern of AT. The scaling factor of 0.95 is used in the O−H stretching region and 0.98 otherwise. The dense bands appearing at 1353, 1344, 1324, and 1311 cm^{-1} are assignable to the most intense band for a mixed mode of in-plane COH bending and C−O stretching, which may be split by the Fermi resonance with a combination band of out-of-plane COH bending, ca. 550 cm^{-1}, and out-of-plane C−H bending, ca. 750 cm^{-1}. Since the calculated spectral pattern reproduces the increasing bands satisfactorily when the above-mentioned splitting is considered, we conclude that SC and ST change to AT by UV irradiation. The observed and calculated wavenumbers and relative intensities of AT are summarized in Table 2.

The spectral changes of the deuterated species in an argon matrix due to UV-induced photoisomerization are also shown in Figure 4c. Most of the observed bands can be assigned to AT by comparison of the observed spectrum with the corresponding calculated spectral pattern in Figure 4d. The strongest band observed at 1298 cm^{-1}, which is split in the spectrum of the normal species, corresponds to the calculated band at 1285 cm^{-1}; the band splitting due to Fermi resonance seems to be avoided by deuteration. The observed and calculated wavenumbers and relative intensities for the deuterated AT are summarized with the results of the normal species in Table 2.

The difference spectrum, Figure 4c, shows additional bands unassigned to AT in the O−D and C═O stretching regions. The 2667 and 1790 cm^{-1} bands correspond to the calculated 2708 and 1806 cm^{-1} bands of deuterated AC shown in Figure 4e, suggesting that another less stable isomer, AC, exists with AT in the matrix after UV irradiation. On the other hand, no IR bands of AC were observed in the spectrum of the normal species, as mentioned above. Hence, we assume that the rate of hydrogen tunneling is so fast that AC changes to SC before the measurement of the IR spectrum but that the rate of deuterium atom tunneling is so slow that the IR bands of AC are observable. Further evidence for the hydrogen tunneling is presented in the next section. The observed and calculated wavenumbers and the relative intensities of deuterated AC are summarized in Table 2. This is the first observation of the less stable isomers of 2-CBA, AT, and AC.

Isomerization Due to Hydrogen Atom Tunneling. When the argon matrix sample was kept in the dark for 300 min after 60 min of UV irradiation ($\lambda > 240$ nm), a spectral change due to isomerization from AT to ST was observed, as shown in Figure 5a. The increasing and decreasing bands in the dark are on the upper and lower sides, respectively. The former is assigned to ST while the latter is assigned to AT on the basis of the vibrational analysis described above.

Three origins for the isomerization from AT to ST in the dark are conceivable: (1) IR-induced isomerization by the IR radiation emitted from an FT-IR spectrophotometer, (2) thermal isomerization over the rotational barrier around the C−OH bond at 9 K, and (3) hydrogen tunneling for the OH group. Origin 1 can be ruled out because the measured isomerization rate was unchanged when the IR beam of the spectrophotometer was cut off before and after the spectral measurement. Origin 2 can also be eliminated, because our DFT calculation of the barrier height for the rotational isomerization around the C−O bond, 32.76 kJ mol^{-1}, is too high to enable thermal isomerization at 9 K.[24] Hence, we ascribe the isomerization from AT to ST to hydrogen tunneling. To confirm this assumption, we compare the isomerization rate constants of normal species with those of deuterated species at various matrix temperatures in argon and xenon matrixes as follows.

Figure 6 shows difference IR spectra in the O−H and O−D stretching regions for the normal and deuterated species in argon matrixes, respectively. The upper spectrum was obtained from the spectra measured after and before 60 min of UV irradiation, where the increasing bands are assigned to AT. When the matrix sample was kept in the dark for 300 min at 9 K, the O−H stretching bands of normal AT, 3487 and 3477 cm^{-1}, decreased with an increase of ST. On the other hand, the intensity of the O−D stretching mode of AT, 2579 cm^{-1}, remained unchanged. These findings suggest a large isotope effect on tunneling isomerization.

A weak band of 2667 cm^{-1} of AC decreased, and a small band of 2630 cm^{-1} of SC increased in the dark. This may also be due to hydrogen tunneling in the carboxyl group. The rate of tunneling for the normal species is too fast to be measurable in the IR bands of AC, but that for the deuterated species is so slow that the IR bands of deuterated AC were observed, as reported above.

To answer the question on whether the Arrhenius plot is linear or nonlinear, the relationship between the isomerization rate in the dark and the matrix temperature was examined by using the total area of the splitting bands for the O−H mode in a Xe matrix. The decays of AT obtained at eight matrix temperatures between 9 and 45 K are plotted in Figure 7, where the observed values are normalized to make the area measured before the sample was placed in the dark unity. As the matrix temperature is higher, the decay rate is larger. In striking contrast, the O−D stretching band of the deuterated species was remarkably unchanged even at 45 K.

The observed data were analyzed by a least-squares fitting by

$$A = (A_0 - A_\infty)\exp(-kt) + A_\infty \qquad (1)$$

TABLE 2: Observed and Calculated Wavenumbers (in cm^{-1}) and Relative Intensities of AT and AC in an Argon Matrix

AT						AC		
normal			deuterated			deuterated		
	calcd[b]			calcd[b]			calcd[b]	
obsd[a]	$\tilde{\nu}$	int	obsd[a]	$\tilde{\nu}$	int	obsd[a]	$\tilde{\nu}$	int
3487, 3477 (s)	3490	51		3068	2		3060	1
	3069	1		3062	0		3051	3
	3062	0		6050	2		3037	1
	3050	2		3037	1		3027	0
	3037	1	2579 (s)	2623	37	2667 (m)	2708	9
1768 (s)	1770	76	1767, 1763 (s)	1765	100	1790 (s)	1806	100
	1607	7	1601 (w)	1607	9		1605	6
	1577	1		1577	2		1581	3
	1468	3	1469 (w)	1468	4		1476	9
1440 (s)	1437	10	1441 (s)	1437	12		1437	7
1353, 1344, 1324, 1311 (s)	1326	100		1311	1	1300, 1294 (m)	1312	9
	1310	0	1298 (s)	1285	99	1275 (m)	1267	18
	1263	1	1252 (m)	1252	12	1256 (s)	1250	79
	1208	2		1166	1		1166	0
	1166	0	1131 (m)	1127	8		1134	4
1118 (s)	1117	3	1117 (m)	1114	5	1114 (m)	1108	29
	1114	4		1042	4		1040	4
	1042	3		1019	7	1053 (m)	1033	25
	1019	6		991	0		981	0
	989	0		965	0		947	1
	965	0	958 (s)	946	6		911	6
	867	0		869	0		865	0
	783	1	788 (w)	776	6		776	11
790 (w)	776	5		773	0		763	3
749 (m)	732	9	746 (s)	732	16		743	17
	684	4	678 (w)	678	6		697	1
	634	1		651	1		679	4
	627	0		628	1		623	3
	541	17		504	0		552	2
	515	0		480	2		466	6
	467	4		439	9		434	6
	441	2		426	4		388	5

[a] The symbols in parentheses represent the relative intensities: s, m, and w denote strong, medium, and weak, respectively. [b] Calculated at the DFT/B3LYP/6-31++G** level. Scaling factors of 0.95 and 0.98 are used in the regions above and below 3000 cm^{-1}, respectively.

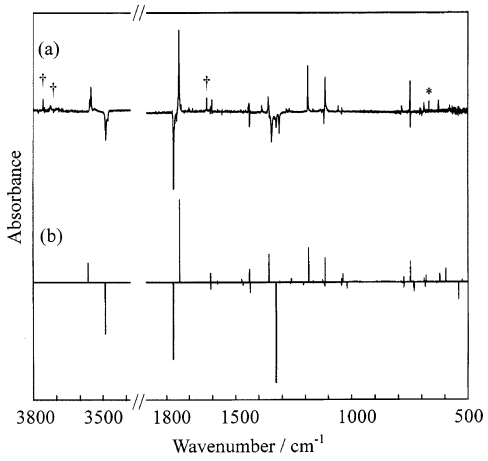

Figure 5. Spectral changes in an argon matrix kept in the dark. (a) Difference spectrum between the spectra measured after and before storage in the dark for 60 min at 9 K subsequent to the 60 min UV irradiation. Bands marked with a dagger and an asterisk are due to H_2O in the matrix and CO_2 in the atmosphere, respectively. (b) Calculated spectral patterns of ST (up) and AT (down).

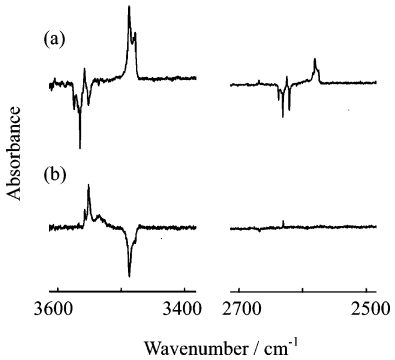

Figure 6. IR bands in the O−H and O−D stretching regions for normal and deuterated 2-chlorobenzoic acid in an argon matrix. (a) Difference spectrum between the spectra measured after and before 60 min of UV irradiation after annealing. (b) Difference spectrum between the spectra measured after and before storage in the dark for 300 min at 9 K after UV irradiation for 60 min.

where A_0 represents the absorbance measured before the sample was placed in the dark. In this kinetic analysis, part of the molecules in the rigid matrix sites were found to remain at infinite time without isomerization. Similar phenomena were sometimes observed in conformational changes in low-temperature rare-gas matrixes.[25] Then we estimated A_∞ as the absorbance of nonreactive species in eq 1. The solid lines drawn in Figure 7 represent the calculated values obtained by a least-squares fitting, where both sides of eq 1 were divided by A_0 for normalization. The calculated values are found to be consistent with the observed values within experimental error. The obtained rate constant, k, and the ratio A_∞/A_0 at the matrix temperature between 9 and 45 K are listed in Table 3. The A_∞/A_0 ratios are smaller at higher matrix temperatures. A probable reason is that the matrix sites inhibiting isomerization are loosened at higher matrix temperatures. On the other hand, the rate constants are larger at higher matrix temperatures. The obtained values for

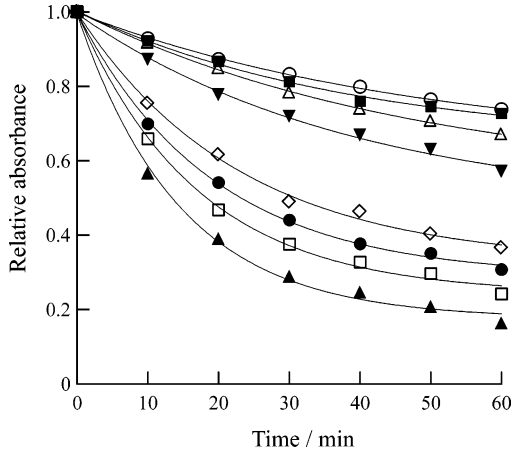

Figure 7. Decaying behaviors of the O−H stretching band (cm^{-1}) of AT in a xenon matrix in the dark. The symbols ○, ■, △, ▼, ◇, ●, □, and ▲ represent the data measured at 9, 12, 15, 20, 30, 35, 40, and 45 K, respectively. The solid curves represent the calculated values obtained by a least-squares fitting.

TABLE 3: Decay Rate Constants (min^{-1}) of AT in a Xenon Matrix[a]

T/K	k/min^{-1}	A_∞/A_0[b]
9	0.020 ± 0.002	0.63 ± 0.02
12	0.025 ± 0.004	0.64 ± 0.03
15	0.021 ± 0.002	0.54 ± 0.02
20	0.025 ± 0.004	0.47 ± 0.04
30	0.043 ± 0.004	0.32 ± 0.02
35	0.052 ± 0.003	0.29 ± 0.01
40	0.059 ± 0.004	0.24 ± 0.02
45	0.069 ± 0.005	0.18 ± 0.02

[a] The uncertainties represent the standard derivations in the least-squares fitting. [b] Ratio of the species in the nonreactive site.

the rate constants were used to confirm the Arrhenius plot, log *k* vs T^{-1}. The relationship between *k* and T^{-1} is found to be nonlinear, as shown in Figure 8. These results lead to the conclusion that the isomerization from AT to ST is caused by hydrogen tunneling as well as the isomerization from AC to SC (see Scheme 3).

4. Summary

Isomerization of 2-chlorobenzoic acid has been studied by low-temperature matrix-isolation IR spectroscopy with the aid of DFT/B3LYP/6-31++G**. The IR spectra of the two stable isomers, SC and ST, were observed after deposition and distinguished from each other by annealing. A less stable isomer,

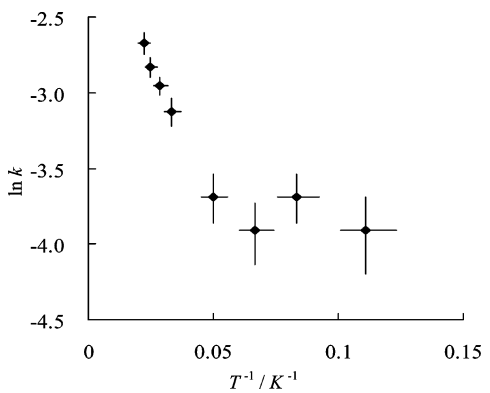

Figure 8. Arrhenius plots of ln *k* against the inverse of the matrix temperature. The error bars represent the standard deviations obtained by a least-squares fitting and ±10% of the matrix temperature.

SCHEME 3

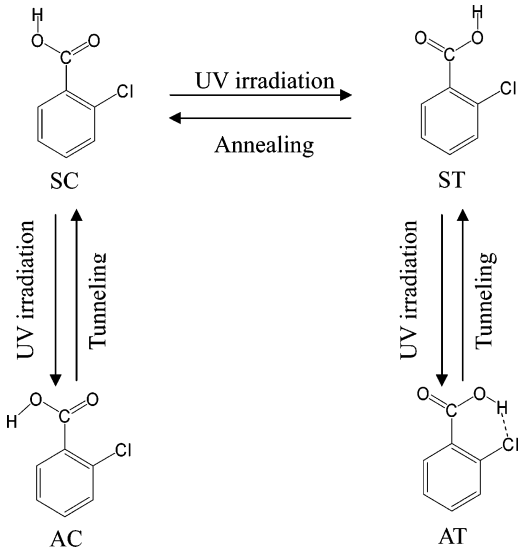

AT, which has a OH···Cl intramolecular hydrogen bond, was produced by UV irradiation. In a deuterated sample, the IR spectra of the least stable isomer, AC, were observed with AT by UV irradiation. When the matrix sample was kept in the dark after UV irradiation, both processes of isomerization, AT → ST and AC → SC, occurred. A drastic H/D isotope effect on the rate of isomerization in the carboxyl group was found. The rate constants of isomerization from AT to ST in a Xe matrix, estimated at various matrix temperatures, showed that the dependence on the matrix temperature deviates from the Arrhenius law. These findings lead to the conclusion that these isomerizations in the dark are caused by hydrogen atom tunneling.

Acknowledgment. We thank Professor Kozo Kuchitsu (BASE, Tokyo University of Agriculture & Technology) for his helpful discussions.

References and Notes

(1) Maçôas, E. M. S.; Khriachtchev, L.; Pettersson, M.; Fausto, R.; Räsänen, M. *Phys. Chem. Chem. Phys.* **2005**, *7*, 743.
(2) Maçôas, E. M. S.; Khriachtchev, L.; Pettersson, M.; Juselius, J.; Fausto, R.; Räsänen, M. *J. Chem. Phys.* **2003**, *119*, 11765.
(3) Maçôas, E. M. S.; Khriachtchev, L.; Pettersson, M.; Lundell, J.; Fausto, R.; Räsänen, M. *Vib. Spectrosc.* **2004**, *34*, 73.
(4) Maçôas, E. M. S.; Khriachtchev, L.; Pettersson, M.; Fausto, R.; Räsänen, M. *J. Am. Chem. Soc.* **2003**, *125*, 16188.
(5) Maçôas, E. M. S.; Khriachtchev, L.; Pettersson, M.; Fausto, R.; Räsänen, M. *J. Chem. Phys.* **2004**, *121*, 1331.
(6) Maçôas, E. M. S.; Khriachtchev, L.; Pettersson, M.; Fausto, R.; Räsänen, M. *J. Phys. Chem. A* **2005**, *109*, 3617.
(7) Akai, N.; Kudoh, S.; Takayanagi, M.; Nakata, M. *Chem. Phys. Lett.* **2002**, *356*, 209.
(8) Akai, N.; Kudoh, S.; Takayanagi, M.; Nakata, *J. Phys. Chem. A* **2002**, *106*, 11029.
(9) Akai, N.; Kudoh, S.; Nakata, M. *J. Phys. Chem. A* **2003**, *107*, 3655.
(10) Kulbida, A.; Nosov, A. *J. Mol. Struct.* **1992**, *265*, 17.
(11) Nieminen, J.; Pettersson, M.; Räsänen, R. *J. Phys. Chem.* **1993**, *97*, 10925.
(12) Fausto, R.; Maçôas, E. M. S.; Kulbida, A. *J. Mol. Struct.* **1999**, *480−481*, 83.
(13) Aarset, K.; Page, E. M.; Rich, D. A. *J. Phys. Chem. A* **2006**, *110*, 9014.
(14) Reva, I. D.; Stepanian, S. G. *J. Mol. Struct.* **1995**, *349*, 337.
(15) Stepanian, S. G.; Reva, I. D.; Radchenko, E. D.; Sheina, G. G. *Vib. Spectrosc*. **1996**, *11*, 123.
(16) Böhm, S.; Fiedler, P.; Exner, O. *New J. Chem.* **2004**, *28*, 67.
(17) Kharitonov, Y. Y.; Oleinik, I. I. *Dokl. Akad. Nauk SSSR* **1987**, *294*, 151.
(18) Akai, N.; Kudoh, S.; Nakata, M. *J. Phys. Chem. A.* **2003**, *107*, 2635.

(19) Futami, Y.; Kudoh, S.; Ito, F.; Nakanaga, T.; Nakata, M. *J. Mol. Struct.* **2004**, *690*, 9.

(20) Frisch, M. J.; Trucks, G. W.; Schlegel, H. B.; Scuseria, G. E.; Robb, M. A.; Cheeseman, J. R.; Montgomery, J. A., Jr.; Vreven, T.; Kudin, K. N.; Burant, J. C.; Millam, J. M.; Iyengar, S. S.; Tomasi, J.; Barone, V.; Mennucci, B.; Cossi, M.; Scalmani, G.; Rega, N.; Petersson, G. A.; Nakatsuji, H.; Hada, M.; Ehara, M.; Toyota, K.; Fukuda, R.; Hasegawa, J.; Ishida, M.; Nakajima, T.; Honda, Y.; Kitao, O.; Nakai, H.; Klene, M.; Li, X.; Knox, J. E.; Hratchian, H. P.; Cross, J. B.; Adamo, C.; Jaramillo, J.; Gomperts, R.; Stratmann, R. E.; Yazyev, O.; Austin, A. J.; Cammi, R.; Pomelli, C.; Ochterski, J. W.; Ayala, P. Y.; Morokuma, K.; Voth, G. A.; Salvador, P.; Dannenberg, J. J.; Zakrzewski, V. G.; Dapprich, S.; Daniels, A. D.; Strain, M. C.; Farkas, O.; Malick, D. K.; Rabuck, A. D.; Raghavachari, K.; Foresman, J. B.; Ortiz, J. V.; Cui, Q.; Baboul, A. G.; Clifford, S.; Cioslowski, J.; Stefanov, B. B.; Liu, G.; Liashenko, A.; Piskorz, P.; Komaromi, I.; Martin, R. L.; Fox, D. J.; Keith, T.; Al-Laham, M. A.; Peng, C. Y.; Nanayakkara, A.; Challacombe, M.; Gill, P. M. W.; Johnson, B.; Chen, W.; Wong, M. W.; Gonzalez, C.; Pople, J. A. *Gaussian 03*, Revision B.04; Gaussian, Inc.: Pittsburgh, PA, 2003.

(21) Beck, A. D. *J. Chem. Phys.* **1993**, *98*, 5648.

(22) Lee, C.; Yang, W.; Parr, R. G. *Phys. Rev. B* **1988**, *37*, 785.

(23) Nandi, C. K.; Samanta, A. K.; Chakraborty, T. *Chem. Phys. Lett.* **2005**, *416*, 261.

(24) Barnes, A. J. *J. Mol. Struct.* **1984**, *113*, 161.

(25) Nagata, M.; Futami, Y.; Akai, N.; Kudoh, S.; Nakata, M. *Chem. Phys. Lett.* **2004**, *392*, 259.